Mean-field approach to nuclear structure with semi-realistic nucleon-nucleon interactions

H. Nakada*
Department of Physics, Graduate School of Science, Chiba University
Yayoi-cho 1-33, Inage, Chiba 263-8522, Japan
(Received 18 September 2008; published 3 November 2008)

Semirealistic nucleon-nucleon interactions applicable to the self-consistent mean-field (both Hartree-Fock and Hartree-Fock-Bogolyubov) calculations are developed by modifying the M3Y interaction. The modification is made to reproduce binding energies and rms matter radii of doubly magic nuclei, single-particle levels in ^{208}Pb and even-odd mass differences of the Sn isotopes. We find parameter sets with and without the tensor force. The new interactions are further checked by the saturation properties of the uniform nuclear matter, including the Landau-Migdal parameters. By the mean-field calculations, interaction dependence of the neutron drip line is investigated for the O, Ca, and Ni isotopes, and of the single-particle energies for the $N = 16, 32, 50$, and 82 and $Z = 50$ nuclei. Results of the semirealistic interactions including the tensor force are in fair agreement with available experimental data for all of these properties.

DOI: 10.1103/PhysRevC.78.054301 PACS number(s): 21.30.Fe, 21.60.Jz, 21.10.Dr, 21.10.Pc

I. INTRODUCTION

Mean-field (MF) theories provide us with a good first approximation to the nuclear structure problems. They are able to describe the saturation and the shell structure simultaneously, both of which are basic nuclear properties, based on effective nucleon-nucleon (NN) interactions. As far as we constrain to the nonrelativistic approaches, most of the MF calculations have been performed with the Skyrme interaction [1]. Finite-range interactions have rarely been applied, except the Gogny interaction [2], which has the Gaussian form for the central channels. Most popular parameter sets of the Skyrme and the Gogny interactions have been adjusted mainly to the nuclear properties around the β stability. However, it is a question whether such phenomenological effective interactions work well for nuclei far off the β stability. For instance, whereas role of the tensor force in nucleus dependence of the MF has attracted interest [3,4], the tensor force is usually ignored in those parameter sets.

Although direct application of the bare NN (and NNN) interaction to the nuclear structure problems [5–7] is yet limited to light nuclei or made to medium-mass nuclei but with limited accuracy, guide from microscopic theories will be valuable even in heavy-mass nuclei. The Michigan three-range Yukawa (M3Y) interaction [8], which was derived by fitting the Yukawa functions to Brueckner's G matrix, has been used in nuclear structure as well as in low-energy nuclear reaction studies. There have been a few attempts applying the M3Y-type interaction to MF calculations [9,10]. In Ref. [10], the author has developed an M3Y-type interaction that is applicable to the Hartree-Fock (HF) calculations. The original M3Y interaction is incapable of reproducing the saturation and the spin-orbit splitting within the MF regime. To cure this problem a density-dependent contact term has been added and some of the strength parameters have been modified. Such interactions, which have originally been derived from microscopic theories but are slightly modified from phenomenological standpoints, may be called *semirealistic* interactions. It has been shown [10,11] that semirealistic NN interactions could give different shell structure from the widely used Skyrme and Gogny interactions. However, the pairing properties have not been taken into account in the parameter-set M3Y-P2 that was proposed in Ref. [10]. This implies that the singlet-even channel in M3Y-P2 is not quite appropriate as long as the pairing interaction is taken to be consistent with the HF interaction, whereas this problem seems to be masked in the HF approximation. To apply semirealistic interactions to the MF studies extensively, we explore new parameter sets of the M3Y-type interaction, taking the pairing properties into account. Special attention is paid also to role of the tensor force. Using the recently developed algorithm [12–14], we apply the new semirealistic interactions to the Hartree-Fock-Bogolyubov (HFB) as well as to the HF calculations of spherical nuclei.

II. M3Y-TYPE INTERACTION

We express a nonrelativistic nuclear effective Hamiltonian by

$$H_N = K + V_N\,; \quad K = \sum_i \frac{\mathbf{p}_i^2}{2M}, \quad V_N = \sum_{i<j} v_{ij}, \qquad (1)$$

with i and j representing the indices of individual nucleons. For the effective NN interaction v_{ij}, we consider the following form,

$$\begin{aligned} v_{ij} &= v_{ij}^{(\mathrm{C})} + v_{ij}^{(\mathrm{LS})} + v_{ij}^{(\mathrm{TN})} + v_{ij}^{(\mathrm{DD})}\,; \\ v_{ij}^{(\mathrm{C})} &= \sum_n \left[t_n^{(\mathrm{SE})} P_{\mathrm{SE}} + t_n^{(\mathrm{TE})} P_{\mathrm{TE}} + t_n^{(\mathrm{SO})} P_{\mathrm{SO}} \right. \\ &\quad \left. + t_n^{(\mathrm{TO})} P_{\mathrm{TO}} \right] f_n^{(\mathrm{C})}(r_{ij}), \\ v_{ij}^{(\mathrm{LS})} &= \sum_n \left[t_n^{(\mathrm{LSE})} P_{\mathrm{TE}} + t_n^{(\mathrm{LSO})} P_{\mathrm{TO}} \right] f_n^{(\mathrm{LS})}(r_{ij})\, \mathbf{L}_{ij} \cdot (\mathbf{s}_i + \mathbf{s}_j), \end{aligned}$$

*nakada@faculty.chiba-u.jp

$$v_{ij}^{(\mathrm{TN})} = \sum_n \left[t_n^{(\mathrm{TNE})} P_{\mathrm{TE}} + t_n^{(\mathrm{TNO})} P_{\mathrm{TO}}\right] f_n^{(\mathrm{TN})}(r_{ij}) r_{ij}^2 S_{ij},$$
$$v_{ij}^{(\mathrm{DD})} = \left\{t_\rho^{(\mathrm{SE})} P_{\mathrm{SE}} \cdot [\rho(\mathbf{r}_i)]^{\alpha^{(\mathrm{SE})}} + t_\rho^{(\mathrm{TE})} P_{\mathrm{TE}} \cdot [\rho(\mathbf{r}_i)]^{\alpha^{(\mathrm{TE})}}\right\} \delta(\mathbf{r}_{ij}), \tag{2}$$

where $\mathbf{r}_{ij} = \mathbf{r}_i - \mathbf{r}_j$, $r_{ij} = |\mathbf{r}_{ij}|$, $\mathbf{p}_{ij} = (\mathbf{p}_i - \mathbf{p}_j)/2$, $\mathbf{L}_{ij} = \mathbf{r}_{ij} \times \mathbf{p}_{ij}$, $S_{ij} = 4\left[3(\mathbf{s}_i \cdot \hat{\mathbf{r}}_{ij})(\mathbf{s}_j \cdot \hat{\mathbf{r}}_{ij}) - \mathbf{s}_i \cdot \mathbf{s}_j\right]$ with $\hat{\mathbf{r}}_{ij} = \mathbf{r}_{ij}/r_{ij}$, and $\rho(\mathbf{r})$ denotes the nucleon density. The Yukawa function $f_n(r) = e^{-\mu_n r}/\mu_n r$ is assumed for all channels except $v^{(\mathrm{DD})}$ in the M3Y-type interactions. The projection operators on the singlet-even (SE), triplet-even (TE), singlet-odd (SO), and triplet-odd (TO) two-particle states are defined as

$$P_{\mathrm{SE}} = \frac{1-P_\sigma}{2}\frac{1+P_\tau}{2}, \quad P_{\mathrm{TE}} = \frac{1+P_\sigma}{2}\frac{1-P_\tau}{2},$$
$$P_{\mathrm{SO}} = \frac{1-P_\sigma}{2}\frac{1-P_\tau}{2}. \quad P_{\mathrm{TO}} = \frac{1+P_\sigma}{2}\frac{1+P_\tau}{2}, \tag{3}$$

where P_σ (P_τ) expresses the spin (isospin) exchange operator.

We shall start from the M3Y-Paris interaction [15], which will be denoted by M3Y-P0 in this article as in Ref. [10]. We change none of the range parameters μ_n of M3Y-P0 in $v^{(\mathrm{C})}$, $v^{(\mathrm{LS})}$, and $v^{(\mathrm{TN})}$. In M3Y-P0, the longest range part in $v^{(\mathrm{C})}$ is kept identical to the central channels of the one-pion exchange potential (OPEP), $v_{\mathrm{OPEP}}^{(\mathrm{C})}$. We also maintain this reasonable assumption. As is well known, the spin-orbit (ℓs) splitting plays a significant role in the nuclear shell structure. Even though higher-order effects may account for the observed ℓs splitting [16], it is desired to enhance $v^{(\mathrm{LS})}$ to describe the shell structure within the MF regime. We here use an overall enhancement factor to $v^{(\mathrm{LS})}$, which is determined from the single-particle spectrum of ^{208}Pb, as will be shown in Sec. IV. Influence of the tensor force on single-particle energies is a current topic, which could be relevant to the new magic numbers in unstable nuclei [3]. We develop two parameter sets having $v^{(\mathrm{TN})}$ without any modification from M3Y-P0, as well as a parameter set in which we impose $v^{(\mathrm{TN})} = 0$.

The saturation properties are important to describe many nuclei in a wide mass range. Because it is still hard to describe accurately the saturation properties by the bare NN (and NNN) interaction despite certain progress [5], it will be appropriate to modify realistic effective interaction to reproduce the saturation properties. Density dependence in the effective interaction has been known to be essential in obtaining the saturation. We therefore add a density-dependent contact force $v^{(\mathrm{DD})}$ [10]. The parameter $\alpha^{(\mathrm{TE})}$ in $v^{(\mathrm{DD})}$, power to ρ, is taken to be 1/3, by which the incompressibility $\mathcal{K}$ becomes close to a reasonable value as shown later. However, $\alpha^{(\mathrm{SE})}$ is not quite sensitive to $\mathcal{K}$, because the major source of the saturation lies in the TE channel, not in the SE channel [17]. Although we simply assumed $\alpha^{(\mathrm{SE})} = \alpha^{(\mathrm{TE})} = 1/3$ in M3Y-P2 [10], this assumption makes it difficult to reproduce pairing properties and to avoid instability of the neutron matter [10,12] simultaneously. To overcome this problem, we adopt $\alpha^{(\mathrm{SE})} = 1$ in the new parameter sets. The difference between $\alpha^{(\mathrm{SE})}$ and $\alpha^{(\mathrm{TE})}$ may be attributed to the difference in origin of the ρ dependence; the short-range repulsion in the bare NN interaction in the SE channel while primarily the tensor force in the TE channel. Validity of the choice $\alpha^{(\mathrm{SE})} = 1$ is further discussed in Sec. III.

The remaining parameters are t_n in $v^{(\mathrm{C})}$ [except those of $v_{\mathrm{OPEP}}^{(\mathrm{C})}$] and t_ρ in $v^{(\mathrm{DD})}$. We fit them to the measured binding energies of ^{16}O and ^{208}Pb, in the HF approximation (see Sec. IV). The proton and neutron Fermi energies of ^{208}Pb, which are primarily relevant to the symmetry energy, are checked additionally. To determine $t_n^{(\mathrm{SE})}$ and $t_\rho^{(\mathrm{SE})}$, we also use the even-odd mass differences of the Sn isotopes, by comparing results of the Hartree-Fock-Bogolyubov (HFB) calculations with the experimental values (see Sec. V). The new parameter-sets of the semirealistic M3Y-type interaction, M3Y-P3 to P5, are tabulated in Table I. For comparison, M3Y-P0 and -P2 are also shown. In the set M3Y-P3, we keep both $v^{(\mathrm{TN})}$ and the odd-channel (SO and TO) strengths in $v^{(\mathrm{C})}$ of M3Y-P0. The set M3Y-P4 is obtained by assuming $v^{(\mathrm{TN})} = 0$, while changing $t_n^{(\mathrm{SO})}$ and $t_n^{(\mathrm{TO})}$ ($n = 1, 2$) substantially. In the set M3Y-P5, we somewhat modify $t_2^{(\mathrm{SO})}$ and $t_2^{(\mathrm{TO})}$ while keeping $v^{(\mathrm{TN})}$, so as to reproduce the binding energies of several doubly magic nuclei better than M3Y-P3, as will be shown in Sec. IV. Thus the number of adjusted parameters are 7, 11, and 9 [including the overall enhancement factor to $v^{(\mathrm{LS})}$] for M3Y-P3, -P4, and -P5, respectively. It will be useful to compare results of these parameter sets for pinning down which part of the interaction is important to individual physical quantities. In particular, the role of the tensor force will be of interest. It is remarked that, although schematic tensor forces have been introduced into some of the recent MF studies [4,18], the present $v^{(\mathrm{TN})}$ in M3Y-P3 and -P5 is much more realistic.

III. PROPERTIES OF NUCLEAR MATTER AT AND AROUND SATURATION POINT

We first view properties of the infinite nuclear matter that are predicted by the semirealistic NN interactions. In the HF approximation, energy of the nuclear matter can be expressed by the following variables:

$$\rho = \sum_{\sigma\tau} \rho_{\tau\sigma},$$
$$\eta_s = \frac{\sum_{\sigma\tau} \sigma \rho_{\tau\sigma}}{\rho} = \frac{\rho_{p\uparrow} - \rho_{p\downarrow} + \rho_{n\uparrow} - \rho_{n\downarrow}}{\rho},$$
$$\eta_t = \frac{\sum_{\sigma\tau} \tau \rho_{\tau\sigma}}{\rho} = \frac{\rho_{p\uparrow} + \rho_{p\downarrow} - \rho_{n\uparrow} - \rho_{n\downarrow}}{\rho}, \tag{4}$$
$$\eta_{st} = \frac{\sum_{\sigma\tau} \sigma\tau \rho_{\tau\sigma}}{\rho} = \frac{\rho_{p\uparrow} - \rho_{p\downarrow} - \rho_{n\uparrow} + \rho_{n\downarrow}}{\rho}.$$

$\rho_{\tau\sigma}$($\tau = p, n$ and $\sigma = \uparrow, \downarrow$, which are sometimes substituted by ± 1 without confusion) stands for densities depending on the spin and the isospin, and is related to the Fermi momentum $k_{F\tau\sigma}$ by

$$\rho_{\tau\sigma} = \frac{1}{6\pi^2} k_{F\tau\sigma}^3. \tag{5}$$

In the interaction of Eq. (2), only $v^{(\mathrm{C})} + v^{(\mathrm{DD})}$ contributes to the energy of the uniform nuclear matter. Formulas to calculate the nuclear matter energy and its derivatives for given $k_{F\tau\sigma}$ have

TABLE I. Parameters of M3Y-type interactions.

Parameters		M3Y-P0	M3Y-P2	M3Y-P3	M3Y-P4	M3Y-P5
$1/\mu_1^{(C)}$	(fm)	0.25	0.25	0.25	0.25	0.25
$t_1^{(SE)}$	(MeV)	11466.	8027.	8027.	8027.	8027.
$t_1^{(TE)}$	(MeV)	13967.	6080.	7130.	5503.	5576.
$t_1^{(SO)}$	(MeV)	−1418.	−11900.	−1418.	−12000.	−1418.
$t_1^{(TO)}$	(MeV)	11345.	3800.	11345.	3700.	11345.
$1/\mu_2^{(C)}$	(fm)	0.40	0.40	0.40	0.40	0.40
$t_2^{(SE)}$	(MeV)	−3556.	−2880.	−2637.	−2637.	−2650.
$t_2^{(TE)}$	(MeV)	−4594.	−4266.	−4594.	−4183.	−4170.
$t_2^{(SO)}$	(MeV)	950.	2730.	950.	4500.	2880.
$t_2^{(TO)}$	(MeV)	−1900.	−780.	−1900.	−1000.	−1780.
$1/\mu_3^{(C)}$	(fm)	1.414	1.414	1.414	1.414	1.414
$t_3^{(SE)}$	(MeV)	−10.463	−10.463	−10.463	−10.463	−10.463
$t_3^{(TE)}$	(MeV)	−10.463	−10.463	−10.463	−10.463	−10.463
$t_3^{(SO)}$	(MeV)	31.389	31.389	31.389	31.389	31.389
$t_3^{(TO)}$	(MeV)	3.488	3.488	3.488	3.488	3.488
$1/\mu_1^{(LS)}$	(fm)	0.25	0.25	0.25	0.25	0.25
$t_1^{(LSE)}$	(MeV)	−5101.	−9181.8	−10712.1	−8671.7	−11222.2
$t_1^{(LSO)}$	(MeV)	−1897.	−3414.6	−3983.7	−3224.9	−4173.4
$1/\mu_2^{(LS)}$	(fm)	0.40	0.40	0.40	0.40	0.40
$t_2^{(LSE)}$	(MeV)	−337.	−606.6	−707.7	−572.9	−741.4
$t_2^{(LSO)}$	(MeV)	−632.	−1137.6	−1327.2	−1074.4	−1390.4
$1/\mu_1^{(TN)}$	(fm)	0.40	0.40	0.40	0.40	0.40
$t_1^{(TNE)}$	(MeV fm^{-2})	−1096.	−131.52	−1096.	0.	−1096.
$t_1^{(TNO)}$	(MeV fm^{-2})	244.	29.28	244.	0.	244.
$1/\mu_2^{(TN)}$	(fm)	0.70	0.70	0.70	0.70	0.70
$t_2^{(TNE)}$	(MeV fm^{-2})	−30.9	−3.708	−30.9	0.	−30.9
$t_2^{(TNO)}$	(MeV fm^{-2})	15.6	1.872	15.6	0.	15.6
$\alpha^{(SE)}$		–	1/3	1	1	1
$t_\rho^{(SE)}$	(MeV fm^3)	0.	181. [a]	220.	248.	126.
$\alpha^{(TE)}$		–	1/3	1/3	1/3	1/3
$t_\rho^{(TE)}$	(MeV fm)	0.	1139.	1198.	1142.	1147.

[a]MeV fm.

been derived in Ref. [10]. Note that, even when superfluidity makes the nuclear matter energy somewhat lower, it is not much different from the energy in the HF approximation.

The spin-saturated symmetric matter is characterized by $\eta_s = \eta_t = \eta_{\rm st} = 0$, for which we denote $k_{F\tau\sigma}$ simply by k_F. The minimum of the energy per nucleon $\mathcal{E} = E/A$, given by

$$\left.\frac{\partial \mathcal{E}}{\partial \rho}\right|_0 = \left.\frac{\partial \mathcal{E}}{\partial k_F}\right|_0 = 0, \tag{6}$$

defines the saturation density ρ_0 (equivalently, k_{F0}) and energy $\mathcal{E}_0$. The expression $|_0$ indicates evaluation at the saturation point. As well as ρ_0 and $\mathcal{E}_0$, second derivatives of $\mathcal{E}$ carry basic information of the effective NN interaction. Two of the curvatures of $\mathcal{E}$ at the saturation point are called incompressibility and volume symmetry energy,

$$\mathcal{K} = k_{\rm F}^2 \left.\frac{\partial^2 \mathcal{E}}{\partial k_F^2}\right|_0 = 9\rho^2 \left.\frac{\partial^2 \mathcal{E}}{\partial \rho^2}\right|_0, \quad a_t = \frac{1}{2}\left.\frac{\partial^2 \mathcal{E}}{\partial \eta_t^2}\right|_0, \tag{7}$$

and are related to the Landau-Migdal (LM) parameters f_0 and f_0' as

$$\mathcal{K} = \frac{3k_{F0}^2}{M_0^*}(1+f_0), \quad a_t = \frac{k_{F0}^2}{6M_0^*}\left(1+f_0'\right), \tag{8}$$

where M_0^* represents the effective mass (k mass) at the saturation point. See Ref. [10] for definition of the LM parameters. The other curvatures of $\mathcal{E}$ with respect to η_s and η_{st}, denoted by a_s and a_{st}, are defined analogously to a_t and are expressed in terms of the LM parameters g_0 and g_0' [10]. The k mass is defined by a derivative of the single-particle

TABLE II. Nuclear matter properties at the saturation point.

		D1S	M3Y-P2	M3Y-P3	M3Y-P4	M3Y-P5
k_{F0}	(fm)	1.342	1.340	1.340	1.340	1.340
$\mathcal{E}_0$	(MeV)	−16.01	−16.14	−16.51	−16.13	−16.12
$\mathcal{K}$	(MeV)	202.9	220.4	245.8	235.3	235.6
M_0^*/M		0.697	0.652	0.658	0.665	0.629
a_t	(MeV)	31.12	30.61	29.75	28.71	29.59
a_s	(MeV)	26.18	21.19	20.17	15.61	19.56
a_{st}	(MeV)	29.13	38.19	36.45	39.89	41.01
$\mathcal{L}_t$	(MeV)	22.44	27.98	25.30	17.87	24.63

energy $\varepsilon(\mathbf{k}\sigma\tau)$:

$$\left.\frac{\partial\varepsilon(\mathbf{k}\sigma\tau)}{\partial k}\right|_0 = \frac{k_{F0}}{M_0^*}, \tag{9}$$

and is connected to the LM parameter f_1 by

$$\frac{M_0^*}{M} = 1 + \frac{1}{3}f_1. \tag{10}$$

In addition, density dependence of the symmetry energy, which is represented by a third derivative of $\mathcal{E}$ as

$$\mathcal{L}_t = \frac{1}{2}k_{\rm F}\left.\frac{\partial^3\mathcal{E}}{\partial k_F\,\partial\eta_t^2}\right|_0 = \frac{3}{2}\rho\left.\frac{\partial^3\mathcal{E}}{\partial\rho\,\partial\eta_t^2}\right|_0, \tag{11}$$

is under interest in relevance to structure of the neutron star crust [19]. These quantities calculated from the new semirealistic interactions are tabulated in Table II. We here set $M = (M_p + M_n)/2$, where M_p (M_n) is the measured mass of a proton (a neutron) [20]. For comparison, the values obtained by the D1S parameter set [21] of the Gogny interaction and from M3Y-P2 are also displayed.

Related to the global systematics of the binding energies and the radii, $k_{F0} \approx 1.33$–$1.34\,\mathrm{fm}^{-1}$ and $\mathcal{E}_0 \approx -16\,\mathrm{MeV}$ have been established empirically. Although the M3Y-P3 interaction yields deeper $\mathcal{E}_0$ than the other interactions, it is still within the range of ambiguity in extracting the volume energy from the experimental data [22]. In practice, M3Y-P3 does not yield overbinding for any of the doubly magic nuclei presented in Sec. IV.

For the incompressibility, $\mathcal{K} \approx 240\,\mathrm{MeV}$ is extracted from the experimental data [23]. The k mass is empirically known to be $M_0^* \approx (0.6 - 0.7)M$ [24]. The volume symmetry energy a_t is important in reproducing global trend of the binding energies for the $Z \neq N$ nuclei, and from empirical viewpoints $a_t \approx 30\,\mathrm{MeV}$ seems appropriate [25]. These are fulfilled reasonably well in all the new parameter sets M3Y-P3 to -P5. The choice $\alpha^{(\mathrm{SE})} = 1$ contributes to the slightly higher $\mathcal{K}$ in M3Y-P3 to -P5 than in D1S and M3Y-P2.

Global characters of the spin and isospin responses are customarily discussed in terms of the LM parameters. By using the formulas given in Ref. [10], we evaluate the LM parameters for the new semirealistic interactions, as shown in Table III. It has been known that g_0 is small, whereas g_0' is relatively large ($\approx$1) [26]. Although the LM parameters should eventually be checked by corresponding excitation modes in actual nuclei, which is beyond the scope of this article, all the semirealistic M3Y-type interactions seem to have reasonable characters on the spin and isospin channels. Not necessarily true for phenomenological interactions such as D1S, this may be linked to the microscopic origin of the interactions. In particular, $v_{\rm OPEP}^{(\mathrm{C})}$ carries about half of g_0' in the results of the M3Y-type interactions [10].

Figure 1 illustrates $\mathcal{E}(\rho)$ for the spin-saturated symmetric nuclear matter obtained from the M3Y-type and the D1S interactions. As pointed out in Ref. [10], difference among the saturating forces is not large at $\rho \lesssim \rho_0$. At relatively high density ($\rho \gtrsim 0.3\,\mathrm{fm}^{-3}$), the M3Y-P3 to -P5 interactions have higher $\mathcal{E}$ than M3Y-P2 and D1S, reflecting higher $\mathcal{K}$. $\mathcal{E}(\rho)$ of M3Y-P4 and -P5 is close to each other even at $\rho \approx 0.6\,\mathrm{fm}^{-3} (\approx 4\rho_0)$.

In Fig. 2, contributions of the SE, TE, SO, and TO channels in $v^{(\mathrm{C})} + v^{(\mathrm{DD})}$ to $\mathcal{E}$ of the symmetric matter are shown as a function of k_F. The contribution of the TE and the SO channels in M3Y-P4 is hard to be distinguished from that in M3Y-P5. So is the contribution of the TE channel in M3Y-P2. The TE channel takes a minimum at $k_F \approx 1.5\,\mathrm{fm}^{-1}$, primarily responsible for the saturation at $k_F = k_{F0} \approx 1.3\,\mathrm{fm}^{-1}$. Both the SO and the TO channels do not contribute to $\mathcal{E}$ significantly at $\rho \lesssim \rho_0$ (i.e., $k_F \lesssim k_{F0}$). Although the SO channel becomes attractive in the D1S interaction, it is repulsive in the M3Y-type

TABLE III. Landau-Migdal parameters at the saturation point.

	D1S	M3Y-P2	M3Y-P3	M3Y-P4	M3Y-P5
f_0	−0.369	−0.357	−0.276	−0.300	−0.336
f_1	−0.909	−1.044	−1.027	−1.005	−1.112
f_2	−0.558	−0.436	−0.355	−0.429	−0.367
f_3	−0.157	−0.210	−0.184	−0.210	−0.182
f_0'	0.743	0.607	0.578	0.538	0.502
f_1'	0.470	0.635	0.670	0.797	0.692
f_2'	0.342	0.245	0.271	0.286	0.267
f_3'	0.100	0.096	0.104	0.106	0.100
g_0	0.466	0.113	0.070	−0.164	−0.007
g_1	−0.184	0.273	0.214	0.374	0.299
g_2	0.245	0.162	0.160	0.190	0.178
g_3	0.091	0.078	0.079	0.085	0.081
g_0'	0.631	1.006	0.933	1.136	1.081
g_1'	0.610	0.202	0.213	0.109	0.087
g_2'	−0.038	0.040	0.063	0.016	0.029
g_3'	−0.036	−0.002	0.005	−0.008	−0.002

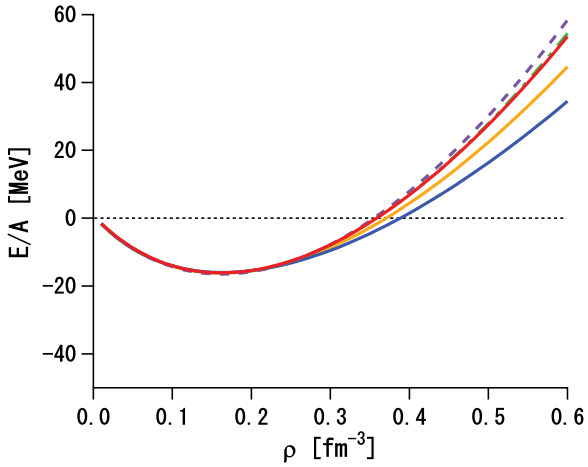

FIG. 1. (Color online) Energy per nucleon $\mathcal{E} = E/A$ in the symmetric nuclear matter for several effective interactions. Purple dashed, green dot-dashed, and red solid lines represent the results with the M3Y-P3, -P4, and -P5 interactions, respectively. Those with the M3Y-P2 and D1S interactions are also displayed for comparison by orange and blue solid lines.

interactions at $\rho > \rho_0$. The TO channel is repulsive in M3Y-P3 and -P5, while attractive in M3Y-P4, although the attraction in M3Y-P4 is not so strong as to cause spin polarization in the pure neutron matter up to $\rho = 1.3\,\mathrm{fm}^{-3} (\approx 8\rho_0)$. Remember that the odd channels in M3Y-P3 are unchanged from M3Y-P0.

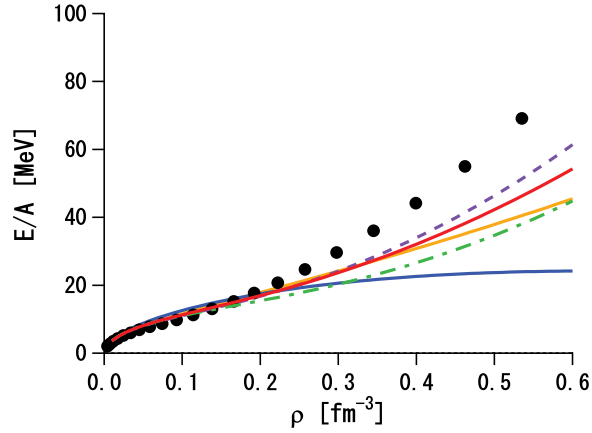

FIG. 3. (Color online) Energy per nucleon $\mathcal{E} = E/A$ in the neutron matter for several effective interactions. Circles are the results of Ref. [27]. See Fig. 1 for the other conventions.

Energy per nucleon in the spin-saturated neutron matter (i.e., $\eta_t = -1$) is presented in Fig. 3. The result from a microscopic calculation in Ref. [27] is also shown as a reference. The unphysical behavior at high ρ in the D1S result, which comes from the absence of density dependence in the SE channel, was pointed out in Refs. [10,12]. The present M3Y-P3 to -P5 interactions have relatively strong ρ dependence at high ρ for the neutron matter, if compared to M3Y-P2 and D1S. This originates in $\alpha^{(\mathrm{SE})} (= 1)$ and tends to make $\mathcal{E}(\rho)$ closer to the result of Ref. [27].

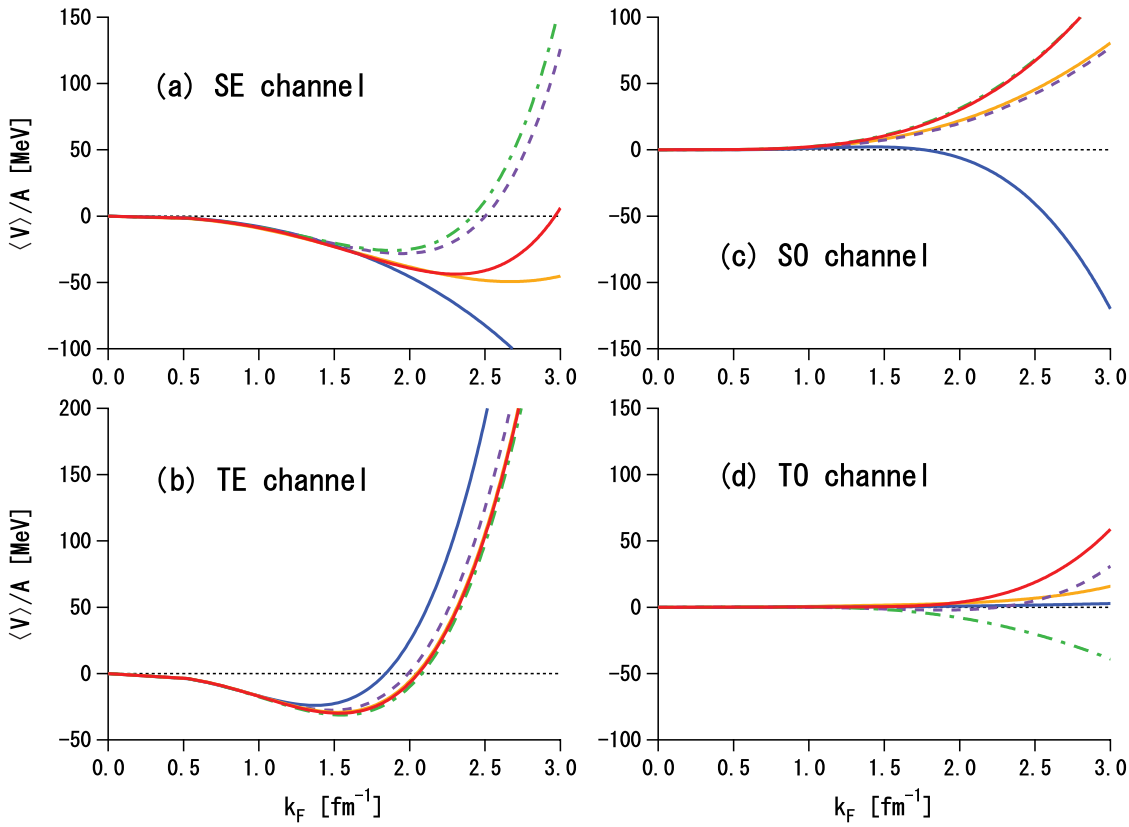

FIG. 2. (Color online) Contribution of the SE, TE, SO, and TO channels to $\mathcal{E}$. See Fig. 1 for conventions.

TABLE IV. Binding energies and rms matter radii of several doubly magic nuclei. Experimental data are taken from Refs. [28–31].

			Exp.	D1S	M3Y-P2	M3Y-P3	M3Y-P4	M3Y-P5
^{16}O	$-E$	(MeV)	127.6	129.5	127.2	118.6	126.3	126.1
	$\sqrt{\langle r^2\rangle}$	(fm)	2.61	2.61	2.61	2.65	2.60	2.59
^{24}O	$-E$	(MeV)	168.5	168.6	165.7	158.2	164.0	166.7
	$\sqrt{\langle r^2\rangle}$	(fm)	3.19	3.01	3.06	3.08	3.04	3.03
^{40}Ca	$-E$	(MeV)	342.1	344.6	338.8	325.2	337.0	335.1
	$\sqrt{\langle r^2\rangle}$	(fm)	3.47	3.37	3.38	3.42	3.37	3.37
^{48}Ca	$-E$	(MeV)	416.0	416.8	411.9	401.0	409.4	414.1
	$\sqrt{\langle r^2\rangle}$	(fm)	3.57	3.51	3.53	3.56	3.52	3.50
^{90}Zr	$-E$	(MeV)	783.9	785.9	779.4	767.9	775.1	779.8
	$\sqrt{\langle r^2\rangle}$	(fm)	4.32	4.24	4.25	4.27	4.24	4.23
^{132}Sn	$-E$	(MeV)	1102.9	1104.1	1099.0	1089.3	1095.7	1098.4
	$\sqrt{\langle r^2\rangle}$	(fm)	–	4.77	4.79	4.81	4.77	4.76
^{208}Pb	$-E$	(MeV)	1636.4	1639.0	1636.5	1635.2	1632.1	1633.2
	$\sqrt{\langle r^2\rangle}$	(fm)	5.49	5.51	5.54	5.55	5.51	5.51

IV. PROPERTIES OF DOUBLY MAGIC NUCLEI

We next turn to doubly magic nuclei, for which the spherical HF approach is expected to be a good approximation.

To all the following calculations of finite nuclei, we apply the recently developed algorithm based on the Gaussian expansion method (GEM) [12,13]. In this method we employ the single-particle bases of

$$\varphi_{\nu\ell jm}(\mathbf{r}) = R_{\nu\ell j}(r)[Y^{(\ell)}(\hat{\mathbf{r}})\chi_\sigma]^{(j)}_m;$$
$$R_{\nu\ell j}(r) = \mathcal{N}_{\nu\ell j}\, r^\ell \exp(-\nu r^2), \tag{12}$$

apart from the isospin index. Here $Y^{(\ell)}(\hat{\mathbf{r}})$ expresses the spherical harmonics and χ_σ the spin wave function. The parameter $\nu = \nu_\mathrm{r} + i\nu_\mathrm{i}$ indicates a complex number corresponding to the range of the Gaussian. Irrespective to nuclide, we adopt the following basis parameters [14]:

$$\nu_\mathrm{r} = \nu_0\, b^{-2n}, \quad \begin{cases} \nu_\mathrm{i} = 0 & (n = 0, 1, \ldots, 5) \\ \frac{\nu_\mathrm{i}}{\nu_\mathrm{r}} = \pm\frac{\pi}{2} & (n = 0, 1, 2) \end{cases}, \tag{13}$$

with $\nu_0 = (2.40\,\mathrm{fm})^{-2}$ and $b = 1.25$ for each (ℓ, j). It is notable that, without parameters specific to mass number or nuclide, a single set of the GEM bases is applicable to wide range of the nuclear mass table [14]. The Hamiltonian is $H = H_N + V_C - H_\mathrm{c.m.}$, where V_C and $H_\mathrm{c.m.}$ represent the Coulomb interaction and the center-of-mass Hamiltonian, while H_N has been given in Eq. (1). The exchange term of V_C is treated exactly, in the same manner as the nuclear force V_N. Both the one- and the two-body terms of $H_\mathrm{c.m.}$ are subtracted before iteration.

The calculated binding energies and rms matter radii of several doubly magic nuclei are displayed in Table IV. The results of the new semirealistic interactions are compared with those of D1S and M3Y-P2 as well as with the experimental data. Influence of the center-of-mass motion on the matter radii is subtracted in a similar manner to the center-of-mass energies [10]. The binding energies of these nuclei obtained from D1S (M3Y-P2) are in agreement with the measured values within the 3 MeV(5 MeV) accuracy. Though the accuracy is slightly worse, the new interactions also reproduce the binding energies moderately well. M3Y-P3 yields underbinding by about 9–17 MeV except for ^{208}Pb. For M3Y-P4 and -P5, maximum deviation in the binding energies shown in Table IV is ∼7 MeV. Because correlations due to the residual interaction could influence, we do not take this deviation seriously at the present stage. The rms matter radii of these nuclei calculated from the semirealistic interactions are comparable to those from the D1S interaction, in fair agreement with the data.

The single-particle levels in ^{208}Pb are depicted in Fig. 4. The levels obtained from M3Y-P5 are compared with those from D1S and the experimental levels. M3Y-P3 and -P4 give single-particle levels similar to, though slightly different from, those of M3Y-P5. The experimental single-particle energies are obtained from the levels of the neighboring nuclei; ^{207,209}Pb, ^{207}Tl, and ^{209}Bi. In the HF results, the overall level spacing is relevant to M_0^* shown in Table II. In the usual HF

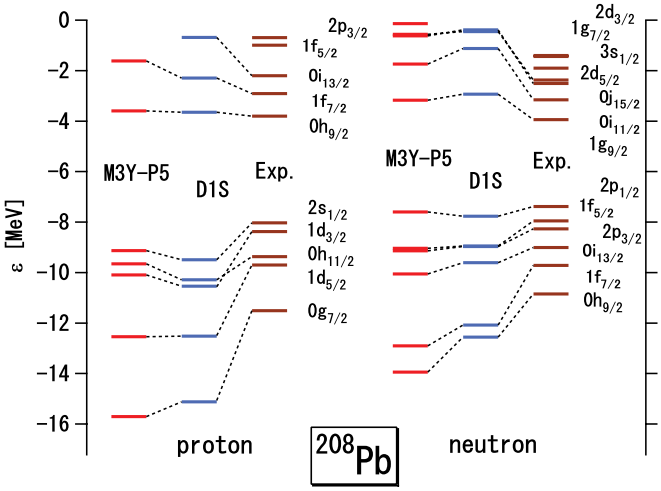

FIG. 4. (Color online) Single-particle energies for ^{208}Pb. Experimental values are extracted from Refs. [31,32].

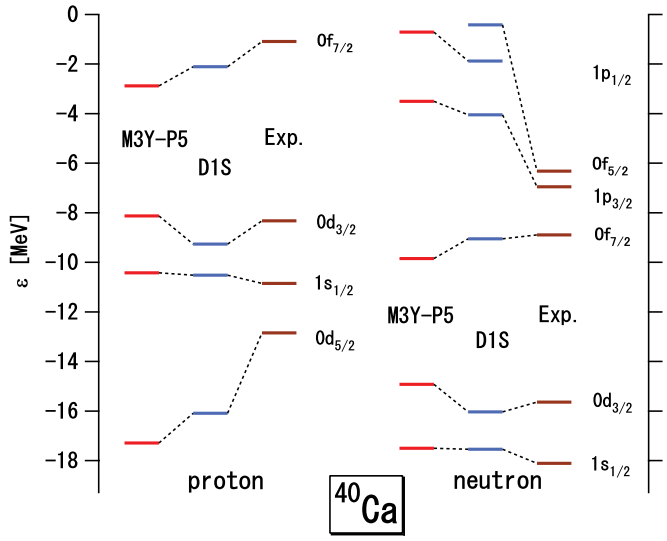

FIG. 5. (Color online) Single-particle energies for ^{40}Ca. Experimental values are extracted from Refs. [31,32].

calculations we have larger level spacing than in the data, and it is not (should not be) remedied until correlations due to the residual interaction (or the ω mass) are taken into account [24]. We thus confirm that the present interactions yield as plausible single-particle levels as D1S does.

In Ref. [4], it has been shown that the $Z = N = 20$ shell gaps are narrowed by the tensor force. It is also true in the M3Y-type interactions. The single-particle energy difference $\varepsilon_\tau(0f_{7/2}) - \varepsilon_\tau(0d_{3/2})$ ($\tau = p, n$) in ^{40}Ca obtained by the D1S interaction is in good agreement with the experimental values, both for protons and neutrons, as viewed in Fig. 5. Although M3Y-P2 and -P4 give almost the same size of the shell gaps as D1S does, we have narrower gaps in the HF calculations with M3Y-P3 and -P5. However, the shell gaps do not collapse by $v^{(\mathrm{TN})}$ of M3Y, in contrast to the zero-range tensor force of Ref. [4]. We still have 5.2 MeV (7.7 MeV) gap for the proton (neutron) orbits with M3Y-P5. These gaps are close to those obtained from the tensor-free Skyrme interaction "T22" in Ref. [4]. It is also worth commenting that, for M3Y-P5, the octupole correlations significantly influence the ground state of ^{40}Ca, as will be discussed elsewhere. This can make the shell gap look wider, having possibility to account for the observed gap.

V. PAIRING PROPERTIES

The M3Y-P2 interaction seems to have reasonable characters in the HF regime, as exemplified in Table IV. However, M3Y-P2 has too strong pair correlations, indicating too strong attraction in the SE channel at low densities though almost invisible in Fig. 2. This character is inherited from the original M3Y interaction. We have developed the M3Y-P3 to -P5 parameter sets by taking the pairing properties into consideration. In this section we shall show characters of the new interactions with respect to the pairing. We restrict ourselves to the pairing among like nucleons, as usual.

We implement the spherical HFB calculations for finite nuclei, using the GEM bases of Eqs. (12) and (13) together with the $\ell \leqslant 7$ truncation. The blocked HFB calculations are applied to the odd-mass nuclei, by assuming that a quasiparticle occupies a specified spherical orbital. When several quasiparticle levels lie closely in energy, we compare the total energies by filling each quasiparticle level and adopt the lowest-energy solution.

A. Even-odd mass difference in Sn isotopes

The $t_n^{(\mathrm{SE})}$ ($n = 1, 2$) and $t_\rho^{(\mathrm{SE})}$ parameters of M3Y-P3 to -P5 are adjusted to the even-odd mass differences of the Sn isotopes with $66 < N < 80$. For the mass difference we use the three-point formula $\Delta^Z_{\mathrm{mass}}(N) = E(Z, N) - \frac{1}{2}[E(Z, N+1) + E(Z, N-1)]$, with $Z = 50$ and $N =$ odd. The mass differences calculated with M3Y-P4 and -P5 are displayed in Fig. 6, in comparison with the experimental data and with those of D1S. Though not shown to keep the figure viewable, M3Y-P3 gives similar $\Delta^{Z=50}_{\mathrm{mass}}(N)$ to M3Y-P4. The calculations are not fully convergent for the ℓ truncation. Moreover, the restoration of the particle-number conservation [33] and the nonspherical mean fields [34] could influence $\Delta^Z_{\mathrm{mass}}(N)$. Each of them could vary $\Delta^Z_{\mathrm{mass}}(N)$ by up to a few hundred keV. Not attempting fine tuning of the parameters, we just point out that some of these effects tend to compensate one another in the mass differences and that the new interactions give $\Delta^{Z=50}_{\mathrm{mass}}(N)$ to comparable accuracy to the D1S interaction in the same model space.

At $N \sim 50, 64$, and 90, we find that the calculated mass differences depend on the interactions. This is ascribed to interaction dependence of the shell structure. Irregularity and discrepancy at $N = 63$ and 65 should be relevant to the $N = 64$ subshell. In M3Y-P5 the subshell effect seems stronger than in the other interactions. At $N \sim 90$ all the M3Y-type interactions yield larger mass differences than D1S. This takes place because $n1f_{7/2}$ and $n2p_{3/2}$ well mix due to the pairing, in the M3Y-type interactions. At $N \sim 50$ M3Y-P5 yields larger mass difference than the other interactions. This is traced back to appreciable excitation from $n1d_{5/2}$ to $n0g_{7/2}$, which takes place because these two orbits are close in energy. Possibly carrying information of the shell structure, data on the masses in $N \sim 50$ and $N \sim 90$ will be of interest.

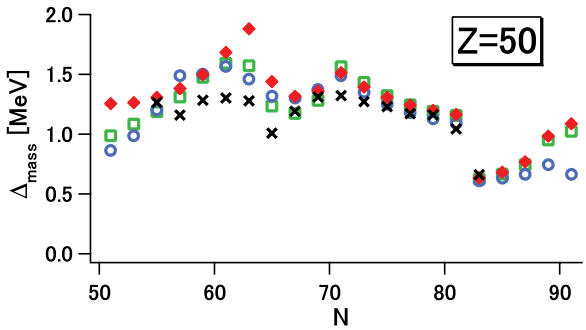

FIG. 6. (Color online) Even-odd mass differences in the Sn isotopes, $\Delta^{Z=50}_{\mathrm{mass}}(N)$. The results of D1S, M3Y-P4 and M3Y-P5 are shown by blue open circles, green open squares and red diamonds, respectively. Experimental values, presented by black crosses, are taken from Ref. [31].

B. Pairing gap in nuclear matter

We next view the pairing property in the nuclear matter obtained from the new semirealistic interactions. In phenomenological studies using the Skyrme energy density functionals, it has been argued [35] whether and how much the pair correlations are dominated by the nuclear surface region. Results of the semirealistic interactions for the nuclear matter may provide certain information on this point. However, we find that, in calculating the pairing properties, the Yukawa function gives quite slow convergence for the maximum momentum of the single-particle states. In practice, even if we cut off the momentum at $k = 50\,\mathrm{fm}^{-1}$, which corresponds to $\varepsilon \approx 50\,\mathrm{GeV}$, the pairing gap is not yet fully convergent. It is impractical to include such high energy states in calculations of finite nuclei. As shown in the preceding subsection, we have fixed the SE channel parameters from the HFB calculations of the Sn nuclei using the basis parameters of Eq. (13). High-momentum components are automatically excluded in the basis set. It will be natural to introduce a certain cutoff in arguing the pairing in the nuclear matter, and the cutoff should desirably be consistent with the basis set of Eq. (13).

The basis set is composed of radial Gaussians whose Fourier transforms are again Gaussians in the momentum space. We here consider a cut-off factor for the single-particle momentum space of

$$g(k) = \theta(k_c - k) + \theta(k - k_c) \exp\left[-\left(\frac{k - k_c}{k_d}\right)^2\right]. \quad (14)$$

The measure in the k integration is multiplied by $g(k)$. Among the bases of Eq. (13), the highest k component is given by the $\nu = \nu_0(1 \pm \frac{\pi}{2}i)$ basis. Because the Fourier transform of this basis is proportional to $\exp[-k^2(1 \pm \frac{\pi}{2}i)/4\nu_0(1 + \frac{\pi^2}{4})]$, $k \lesssim k_0 = 2\sqrt{\nu_0(1+\frac{\pi^2}{4})} (\approx 1.55\,\mathrm{fm}^{-1})$ components are well included in the set. To be consistent with the basis set, it will be reasonable to take $k_c \sim k_0$ for the nuclear matter calculation. We here consider three cases, $(k_c, k_d) = (k_0, k_0)$, $(2k_0, k_0)$, and $(4\,\mathrm{fm}^{-1}, 0)$. The last choice of the $k_d \to 0$ limit indicates a sharp cutoff, and $k_c = 4\,\mathrm{fm}^{-1}$ approximately corresponds to the maximum quasiparticle energy in the HFB calculations of the Sn nuclei.

In Fig. 7, the pairing gap at the Fermi energy, which is obtained from the Bardeen-Cooper-Schrieffer (BCS) calculation in the symmetric nuclear matter using the method of Ref. [36], is plotted as a function of $k_F = (3\pi^2\rho/2)^{1/3}$. The pairing among like nucleons arises from the SE channel in the effective interaction. The result of the M3Y-P5 interaction is compared with that of the Gogny D1S interaction. The cutoff is not needed for the Gogny interaction, and the present cut-off does not influence the D1S gap. The pairing gaps of M3Y-P3 and -P4 are similar to that of M3Y-P5.

The new semirealistic interactions are not drastically different from D1S, in respect to the pairing properties in the nuclear matter. The gap has a peak at $k_F \approx 0.8\,\mathrm{fm}^{-1} \approx 0.6k_{F0}$, namely at $\rho \approx 0.2\rho_0$, for all cases. However, the peak height and the behavior at $\rho > 0.2\rho_0$ are different between the M3Y-type interactions and D1S. With rapid decrease at $\rho > 0.2\rho_0$, the M3Y-type interactions have more surface-dominant pairing

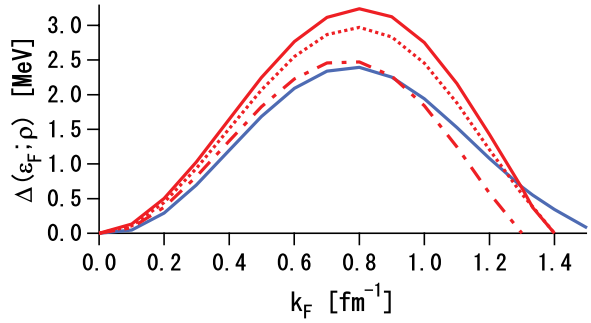

FIG. 7. (Color online) Pairing gap at the Fermi level ε_F in the symmetric nuclear matter. Red dot-dashed, solid, and dotted curves are obtained from M3Y-P5 with the momentum cutoff $(k_c, k_d) = (k_0, k_0)$, $(2k_0, k_0)$ and $(4\,\mathrm{fm}^{-1}, 0)$ in Eq. (14), respectively. Blue solid curve displays gap of the D1S interaction.

than D1S. In D1S, the pair correlation may have sizable contribution from the bulk, even though it is stronger at the nuclear surface. Note that the cut-off parameter does not influence the nuclear matter pairing qualitatively, as long as it is more or less harmonious with the basis set adopted in the calculations of finite nuclei.

VI. NEUTRON DRIP LINE

Prediction of the neutron drip line depends on effective interactions to a certain degree. In this section we compare location of the neutron drip line predicted by the spherical HFB calculations with the present semirealistic interactions and with the Gogny D1S interaction for the O, Ca, and Ni isotopes. Although complete description of the drip line may require fine tuning of the parameters as well as taking account of correlation effects, it will be interesting to see what is relevant to location of the drip line.

A. $Z = 8$ nuclei

We present the two-neutron separation energies S_{2n} for the O isotopes in Fig. 8. The calculated values are compared with the experimental data. We do not show S_{2n} if the neutron chemical potential is positive. Though not displayed in Fig. 8, S_{2n} obtained from M3Y-P3 is close either to that from D1S or M3Y-P4. Whereas $^{25-28}$O have experimentally been established to be unbound [37], most MF calculations so far have failed to reproduce this nature. It would be noteworthy that one of the present semirealistic interactions, M3Y-P5, correctly describes the location of the neutron drip line for oxygen within the spherical HFB approximation; ^{24}O is the heaviest bound oxygen isotope. The ^{25}O nucleus has higher energy than ^{24}O, and in $^{26-28}$O the chemical potential becomes positive. In contrast, ^{26}O is bound in the HFB calculations with M3Y-P3 and P4, as in the calculation with the D1S interaction.

The reason why ^{26}O is not bound with M3Y-P5 can be traced back to $\varepsilon_n(0d_{3/2})$, the single-particle energy of $n0d_{3/2}$. In Fig. 9, the neutron single-particle energies in the HF calculations are depicted. We show the energies obtained from

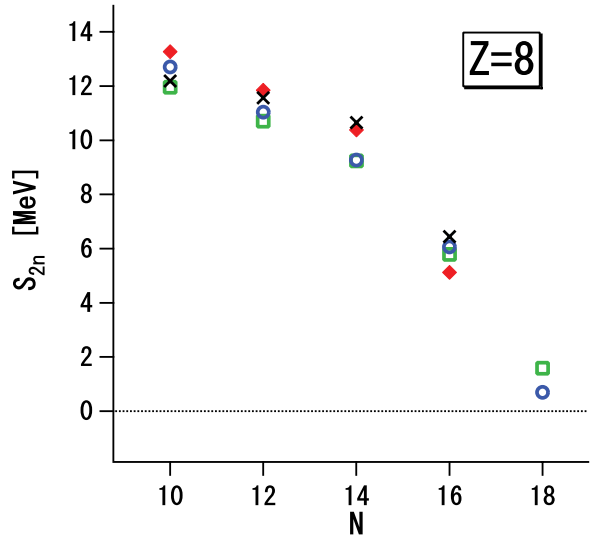

FIG. 8. (Color online) S_{2n} of the O isotopes (N = even). The calculations are performed in the spherical HFB approximation. Experimental data are taken from Ref. [31]. See Fig. 6 for conventions.

the bases of Eq. (13) even when the single-particle energy is positive, not treating the boundary condition carefully. We view that M3Y-P5 gives higher $\varepsilon_n(0d_{3/2})$ than the other interactions, which originates from the slightly stronger $v^{(\mathrm{LS})}$ as well as from the relatively small M_0^*. Note that we have fixed the enhancement factor for $v^{(\mathrm{LS})}$ in M3Y-P5 so as to reproduce the single-particle spectrum around ^{208}Pb, not adjusting accurately to, e.g., the ℓs splitting around ^{16}O. It is commented that $v^{(\mathrm{TN})}$ has small but attractive contribution to $\varepsilon_n(0d_{3/2})$, and therefore is irrelevant to the higher $\varepsilon_n(0d_{3/2})$ in the M3Y-P5 result.

B. $Z = 20$ and 28 nuclei

Location of the neutron drip line for the Ca and Ni nuclei could be investigated by the currently constructed or designed experimental facilities [38]. We tabulate location of the neutron drip line predicted by the spherical HFB calculations with the M3Y-type and the D1S interactions, in Table V.

TABLE V. Neutron numbers of the heaviest bound Ca and Ni nuclei predicted by the spherical HFB calculations with several interactions.

Isotope	D1S	M3Y-P3	M3Y-P4	M3Y-P5
Ca	44	50	48	50
Ni	58	64	62	60

If we use the D1S interaction, the heaviest bound Ca nucleus is ^{64}Ca, because the neutron chemical potential is positive in $N \geqslant 45$. The M3Y-P3 and -P5 interactions predict that ^{70}Ca is bound, whereas ^{68}Ca is the heaviest bound Ca isotope in the M3Y-P4 result. We depict difference between the HF and the HFB energies for the Ca nuclei in Fig. 10, which represents the pair correlation. Though not shown, M3Y-P3 gives similar results to M3Y-P5. While the pairing effects are in good agreement among all of these interactions in $N \leqslant 32$, the M3Y-type interactions give stronger pairing than D1S in $N \geqslant 34$.

Both in the predicted position of the neutron drip line and in the pair correlation in $N \geqslant 34$, the single-particle energy of $n0g_{9/2}$ plays an important role. The neutron drip line can extend up to ^{70}Ca if $\varepsilon_n(0g_{9/2})$ is sufficiently low. At ^{60}Ca we have $\varepsilon_n(0g_{9/2}) = +0.73, -0.63, +0.23$, and -0.65 MeV in the HF calculations with D1S and M3Y-P3, -P4, and -P5, respectively, well correlated to the location of the drip line. The lower $\varepsilon_n(0g_{9/2})$ leads to the smaller shell gap at $N = 40$, $\varepsilon_n(0g_{9/2}) - \varepsilon_n(0f_{5/2})$, which makes the pair excitation across $N = 40$ easier. The gap is 3.8, 2.0, 3.7, and 1.7 MeV in D1S and M3Y-P3, -P4, and -P5. It is noted that this quenching of the shell gap in M3Y-P3 and -P5 comes from the relatively strong $v^{(\mathrm{LS})}$ to some degree, but not from $v^{(\mathrm{TN})}$, because $v^{(\mathrm{TN})}$ hardly contributes to the single-particle energies in an ℓs-closed shell.

The vanishing difference between the HF and HFB energies is often connected to the shell (or subshell) closure. Figure 10

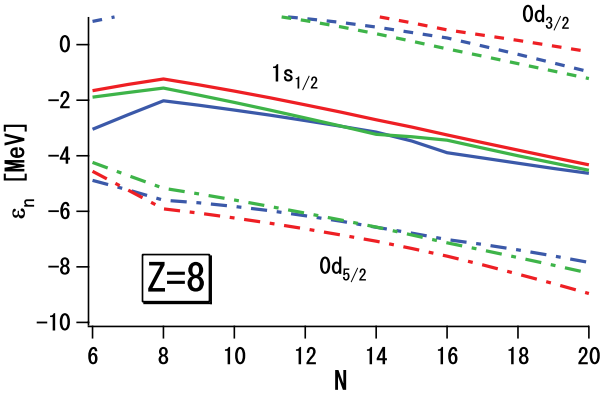

FIG. 9. (Color online) HF single-particle energies in the O isotopes. Blue, green, and red lines represent the results with the D1S, M3Y-P4, and M3Y-P5 interactions, respectively. For each interaction, dot-dashed line is for $\varepsilon_n(0d_{5/2})$, solid line for $\varepsilon_n(1s_{1/2})$ and dashed line for $\varepsilon_n(0d_{3/2})$.

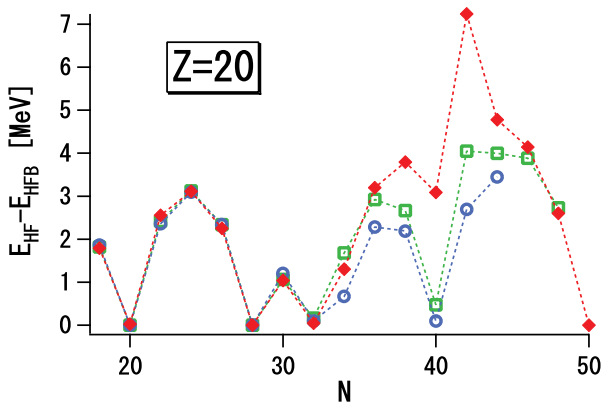

FIG. 10. (Color online) Difference between the HF and HFB energies for the Ca isotopes (N = even), obtained from D1S, M3Y-P4, and -P5. See Fig. 6 for conventions. Dotted lines are drawn to guide eyes.

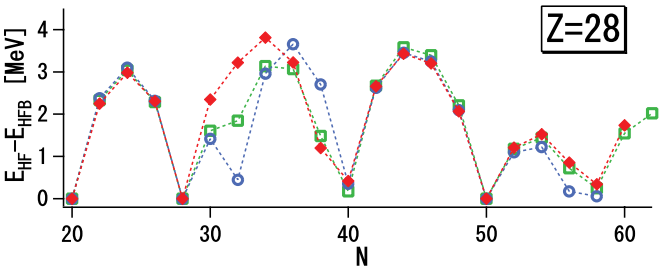

FIG. 11. (Color online) Difference between the HF and HFB energies for the Ni isotopes (N = even). See Fig. 6 for conventions.

indicates that, although ^{60}Ca is stiff against the pair excitation with D1S and M3Y-P4, significant pair excitation occurs by M3Y-P5 (and by M3Y-P3), because of the small shell gap at $N = 40$. On the contrary, $N = 50$ is stiff against the pair excitation in the present M3Y-P3 and -P5 results, in which ^{70}Ca is bound. We have $\varepsilon_n(0g_{9/2}) \approx -2$ MeV at ^{70}Ca, and the gap between $n0g_{9/2}$ and the continuum seems large enough for $N = 50$ to keep the magic nature against the pairing, if we use the present semirealistic pairing interaction. Figure 10 also suggests shell closure at $N = 32$. We shall return to this point in Sec. VII.

In Fig. 11, difference between the HF and HFB energies is shown for the Ni isotopes. For all the interactions, the energy difference becomes vanishingly small at $N = 20, 28, 40, 50$, and 58. We view significant interaction dependence in $28 < N < 40$. In particular, the pair correlation is suppressed at $N = 32$ with D1S, whereas no such effect is found with M3Y-P5. It is noted that, with M3Y-P5, ^{68}Ni seems almost doubly magic as is consistent with experiments [39], although ^{60}Ca is not, as has been seen in Fig. 10. For the neutron-rich Ni region, energy sequence of the single-particle orbitals above $N = 50$ is $1d_{5/2}$, $2s_{1/2}$, $1d_{3/2}$, and $0g_{7/2}$, from the lower orbit to the higher. The hindrance of the pair excitation at ^{86}Ni suggests magic or submagic nature of $N = 58$ due to the gap between $n2s_{1/2}$ and $n1d_{3/2}$. Unlike the M3Y-type interactions, by D1S the pair excitation is hindered also at $N = 56$. The predicted neutron drip line appreciably depends on $\varepsilon_n(1d_{3/2})$ and $\varepsilon_n(0g_{7/2})$. The D1S interaction yields higher $\varepsilon_n(1d_{3/2})$ than the M3Y-type interactions, which causes the drip line at $N = 58$. The low $\varepsilon_n(0g_{7/2})$ in M3Y-P3 induces pair excitation to $0g_{7/2}$, leading to the binding up to ^{92}Ni.

In the highly neutron-rich region, the diffuseness of the nuclear surface becomes larger than in the β-stable region. Then the pair correlation could be relatively strong if it has the surface-dominant nature. However, it is not easy to argue precisely the extent of surface dominance in the pairing from location of the drip line, because it is obscured by influence of the shell structure. In practice, when we use M3Y-P5 for the HF Hamiltonian and D1S for the pair potential, predicted location of the drip line for Ca is the same as the result of the pure M3Y-P5 prediction. For the Ni case, although ^{88}Ni becomes unbound when D1S is used for the pair potential, the chemical potential is only -0.07 MeV in the pure M3Y-P5 result. It will be fair to say that the difference in the pairing channel between the M3Y-type interactions and D1S is not quite significant to location of the neutron drip line. Dependence of the rms matter radii on the pairing interaction is not apparent either, as long as we work with the present M3Y-type or the D1S interactions, whereas the radii near the drip line are sensitive to the separation energies.

VII. NUCLEUS DEPENDENCE OF SINGLE-PARTICLE ENERGIES

It has been pointed out that the shell structure, particularly its nucleus-dependence (sometimes called *shell evolution*), may be connected to characters of effective interactions [3,10,40]. In recent studies role of the tensor force in the shell structure has attracted great interest [3,4]. It is known that observed energies of one-particle states on top of a certain core are appreciably disturbed by correlations beyond the MF regime. However, it is presumable that those correlations do not vary in a certain region of nuclei. In the Sb and the $N = 83$ nuclei, single-particle energies of a few orbitals are extracted from several fragmented states [41], by averaging their energies weighted by the spectroscopic factors. As a result, the averaged single-particle energies are shifted from the lowest states with specific spin-parity nearly by a constant, from nucleus to nucleus. Although data on the averaged energies are not available in many cases, we proceed to investigate nucleus dependence of the shell structure by using the measured energies of the lowest states.

In this section we shall investigate nucleus-dependence of single-particle energies, using the spherical HF or HFB calculations. Results of several interactions are compared. In the HF calculations for open-shell nuclei, the HF Hamiltonian is obtained by folding the interaction by the occupation numbers on each spherical orbital up to the Fermi level.

A. Neutron orbits and shell gap in $N = 16$ nuclei

Nucleus dependence of single-particle energies could be relevant to the new magic numbers in unstable nuclei [3,40]. We investigated the single-particle energies in the $N = 16$ and 32 nuclei in Refs. [10,11] and disclosed role of $v_{\rm OPEP}^{\rm (C)}$ for the $N = 16$ isotones, using the M3Y-P2 interaction. We shall reinvestigate nucleus dependence of the single-particle energies in these nuclei, drawing attention also to the tensor force.

Z dependence of the neutron single-particle energy $\varepsilon_n(0d_{3/2})$ relative to $\varepsilon_n(1s_{1/2})$ is appreciably affected by effective interactions [10,42]. Figure 12 depicts $\Delta\varepsilon_n = \varepsilon_n(0d_{3/2}) - \varepsilon_n(1s_{1/2})$ for varying Z obtained from the HF calculations in the $N = 16$ isotones. Though not shown, $\Delta\varepsilon_n$ of M3Y-P3 resembles that of M3Y-P5. To clarify role of $v^{\rm (TN)}$ and $v_{\rm OPEP}^{\rm (C)}$, we also plot their contributions to $\Delta\varepsilon_n$ in the M3Y-P5 result, which are calculated as $\sum_{j'}\langle N_{j'}\rangle(2J+1)\langle jj'J|v|jj'J\rangle/(2j+1)(2j'+1)$ and shifted by the values at $N = 14$.

The present semirealistic interactions yield increasing $\Delta\varepsilon_n$ as Z goes from 14 to 8, in contrast to the D1S interaction. We view in Fig. 12 that $v_{\rm OPEP}^{\rm (C)}$ [42] and $v^{\rm (TN)}$ produce this feature cooperatively. This Z dependence of the single-particle energies could be relevant to the new magic number $N = 16$ in the neutron-rich region [43]. It has been confirmed that

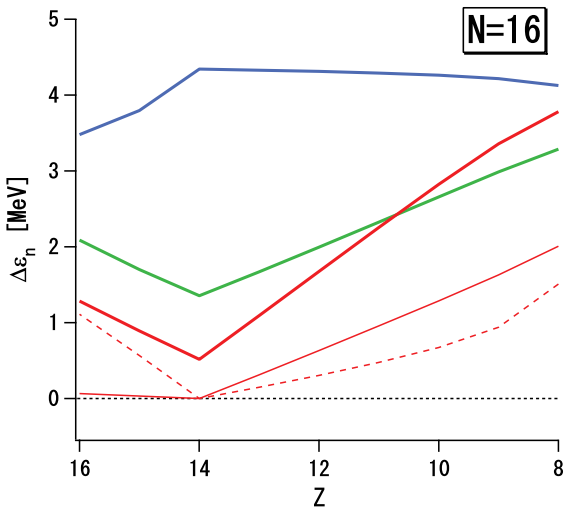

FIG. 12. (Color online) $\Delta\varepsilon_n = \varepsilon_n(0d_{3/2}) - \varepsilon_n(1s_{1/2})$ for the $N = 16$ isotones. Blue, green, and red lines correspond to the results with the D1S, M3Y-P4, and P5 interactions, respectively. Thin red solid and dashed lines represent relative contributions of $v^{(\mathrm{TN})}$ and $v^{(\mathrm{C})}_{\mathrm{OPEP}}$ in the M3Y-P5 result.

several popular Skyrme interactions show similar behavior to D1S [42].

B. Neutron orbits and shell gap in $N = 32$ nuclei

In Fig. 13, Z dependence of the neutron single-particle energies relative to $\varepsilon_n(1p_{3/2})$, $\Delta\varepsilon_n(j) = \varepsilon_n(j) - \varepsilon_n(1p_{3/2})$, is shown for the $N = 32$ nuclei, by taking $j = 0f_{5/2}$ and $1p_{1/2}$. As in the preceding subsection, contributions of $v^{(\mathrm{TN})}$ and $v^{(\mathrm{C})}_{\mathrm{OPEP}}$ to $\Delta\varepsilon_n(0f_{5/2})$ in the M3Y-P5 result are also presented, after shifting by the values at $Z = 28$. With the M3Y-P5 interaction we obtain strong Z dependence in $\Delta\varepsilon_n(0f_{5/2})$,

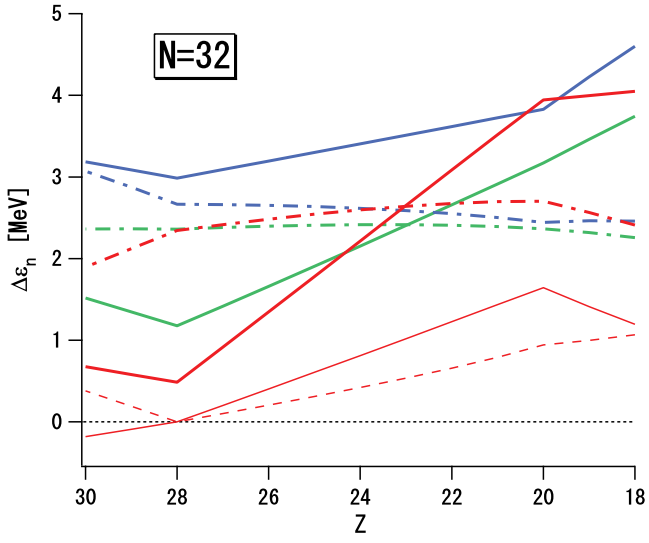

FIG. 13. (Color online) $\Delta\varepsilon_n(0f_{5/2}) = \varepsilon_n(0f_{5/2}) - \varepsilon_n(1p_{3/2})$ (solid lines) and $\Delta\varepsilon_n(1p_{1/2}) = \varepsilon_n(1p_{1/2}) - \varepsilon_n(1p_{3/2})$ (dot-dashed lines) for the $N = 32$ isotones. See Fig. 12 for conventions of colors. Thin red solid and dashed lines represent relative contributions of $v^{(\mathrm{TN})}$ and $v^{(\mathrm{C})}_{\mathrm{OPEP}}$ to $\Delta\varepsilon_n(0f_{5/2})$ in the M3Y-P5 result.

which could be relevant to the magicity of $N = 32$ in the neutron-rich region [44]. Once again this Z dependence originates in $v^{(\mathrm{C})}_{\mathrm{OPEP}}$ [11] and $v^{(\mathrm{TN})}$.

This behavior of $\Delta\varepsilon_n(0f_{5/2})$ is reflected in the pair correlations shown in Figs. 10 and 11. The pairing effects are small at $N = 32$ for all the interactions in the calcium case, because $\Delta\varepsilon_n(0f_{5/2})$ as well as $\Delta\varepsilon_n(1p_{3/2})$ are greater than 2 MeV. Recall that this single-particle energy difference competes with the pairing gap, whose typical value is estimated to be $\Delta \approx 12A^{-1/2} \approx 1.7$ MeV. However, in the nickel case the narrow $\Delta\varepsilon_n(0f_{5/2})$ leads to substantial pair excitation at $N = 32$ for the M3Y-type interactions, whereas such excitation is kept suppressed in the D1S result.

In the neutron-rich region of $Z \sim 20$, there was a prediction that $N = 34$ should be a magic number, based on a shell-model calculation [45]. The present MF calculations with the semirealistic interactions do not support this prediction. Although the $N = 32$ shell gap is 2.7 MeV for ^{52}Ca in the HF calculation with M3Y-P5, the $N = 34$ gap is only 1.2 MeV for ^{54}Ca. The pair excitation across $N = 34$ is sizable, as has been viewed in Fig. 10.

C. Proton orbits in $Z = 50$ nuclei

In recent studies, nucleus dependence of single-particle energies in the Sn isotopes and in the $N = 82$ isotones has been disclosed from experiments [41]. It has been pointed out that the tensor force seems to play a crucial role in the N dependence of the proton single-particle energies in the Sn isotopes [18]. We now have the M3Y-type interactions with quite realistic tensor force (M3Y-P3 and -P5) and without tensor force (M3Y-P4), both of which reproduce the properties of doubly magic nuclei as well as the pairing properties to reasonable accuracy. We apply the HFB calculations with these new interactions to investigating the nucleus dependence of the single-particle energies in the Sn nuclei in this subsection, and in the $N = 50$ and $N = 82$ nuclei in the subsequent subsection.

In the previous studies [18,41], the relative proton single-particle energies $\varepsilon_p(0h_{11/2}) - \varepsilon_p(0g_{7/2})$ were the point of discussion. We here consider the energies of these two orbits relative to $1d_{5/2}$, $\Delta\varepsilon_p(j) = \varepsilon_p(j) - \varepsilon_p(1d_{5/2})$ with $j = 0g_{7/2}$ and $0h_{11/2}$. Taking $\Delta\varepsilon_p(j)$ at $N = 64$ to be a reference and denoting it by $\Delta\varepsilon^0_p(j)$, we plot $\delta\Delta\varepsilon_p(j) = \Delta\varepsilon_p(j) - \Delta\varepsilon^0_p(j)$ in Fig. 14. The values of the M3Y-type interactions (M3Y-P4 and -P5) are presented together with those of D1S and the experimental data. For the data we use the energies of the lowest states in the Sb nuclei.

The semirealistic M3Y-P5 interaction reproduces $\delta\Delta\varepsilon_p(j)$ remarkably well. In the $64 \leqslant N \leqslant 82$ region, the N dependence of $\Delta\varepsilon_p(j)$ takes place due primarily to the occupation of $n0h_{11/2}$, to which contribution of $v^{(\mathrm{TN})}$ is significant. Though not shown, $\delta\Delta\varepsilon_p(j)$ with M3Y-P3 is close to the M3Y-P5 result. With D1S, whereas $\delta\Delta\varepsilon_p(0g_{7/2})$ is in qualitative agreement with the data, $\delta\Delta\varepsilon_p(0h_{11/2})$ is not, because the tensor force is absent. The same holds for M3Y-P4. Although M3Y-P4 reproduces the tendency of the observed N dependence of $\varepsilon_p(0h_{11/2}) - \varepsilon_p(0g_{7/2})$, it gives wrong behavior for $\delta\Delta\varepsilon_p(0h_{11/2})$; i.e., N dependence of $\varepsilon_p(0h_{11/2})$ relative to $\varepsilon_p(1d_{5/2})$. It is also remarked that M3Y-P5 gives quite different

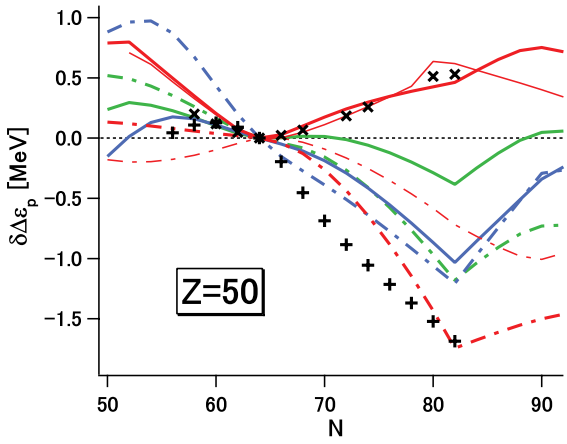

FIG. 14. (Color online) $\delta\Delta\varepsilon_p(j)$ in the Sn isotopes (N = even) for $j = 0g_{7/2}$ (dot-dashed lines) and $0h_{11/2}$ (solid lines). Blue, green, and red lines represent the results of D1S, M3Y-P4, and M3Y-P5, as before. Pluses ($j = 0g_{7/2}$) and crosses ($j = 0h_{11/2}$) are experimental values taken from the lowest states of the Sb nuclei [32]. Thin red lines are contributions of $v^{(\mathrm{TN})}$ in the single-particle levels of M3Y-P5.

behavior of $\delta\Delta\varepsilon_p(j)$ from D1S and M3Y-P4 in $N < 64$, and that the currently available data favor the result of M3Y-P5. We have confirmed that $v^{(\mathrm{C})}_{\mathrm{OPEP}}$ does not have important effects on the N dependence of $\Delta\varepsilon_p(j)$.

It is emphasized that the M3Y-P5 interaction can reproduce the variation of the single-particle energy difference in the Sn isotopes without destroying the shell structure of the doubly magic nuclei shown in Sec. IV. This could be an advantage of the present realistic tensor force. In Ref. [4], no such parameters were found within the Skyrme density functional including the zero-range tensor force.

D. Neutron orbits in $N = 50$ and $N = 82$ nuclei

In the preceding subsection, we have seen that the tensor force affects $\varepsilon_p(0g_{7/2})$ and $\varepsilon_p(0h_{11/2})$ via the occupation of $n0h_{11/2}$. This is accounted for by the attractive (repulsive) nature of the tensor force between a neutron occupying a $j_> =$

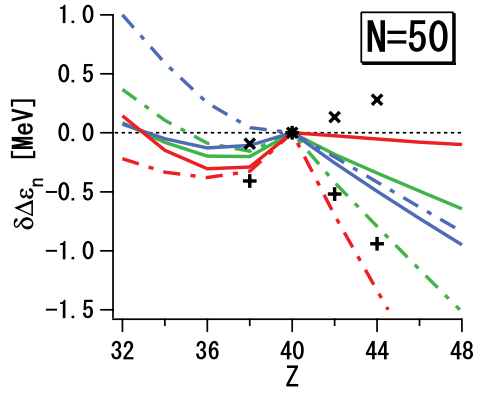

FIG. 15. (Color online) $\delta\Delta\varepsilon_n(j)$ in the $N = 50$ isotones (Z = even), for $j = 0g_{7/2}$ and $0h_{11/2}$. Conventions are the same as in Fig. 14, except that j represents the neutron orbits and $Z = 40$ is taken to be a reference. Experimental values are taken from the lowest states of the $N = 51$ nuclei [32].

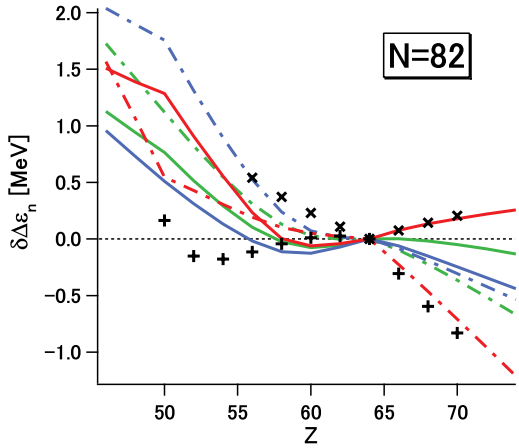

FIG. 16. (Color online) $\delta\Delta\varepsilon_n(j)$ in the $N = 82$ isotones (Z = even), for $j = 0h_{9/2}$ (dot-dashed lines), and $0i_{13/2}$ (solid lines). See Fig. 14 for conventions of colors. Pluses ($j = 0h_{9/2}$) and crosses ($j = 0i_{13/2}$) are experimental values taken from the lowest states of the $N = 83$ nuclei [32].

$\ell + 1/2$ orbit and a proton occupying $j'_< = \ell' - 1/2 (j'_> = \ell' + 1/2)$ [18]. The same mechanism is expected for $\varepsilon_n(0g_{7/2})$ and $\varepsilon_n(0h_{11/2})$ in the $N = 50$ nuclei, as $p0g_{9/2}$ is occupied. We define $\Delta\varepsilon_n(j) = \varepsilon_n(j) - \varepsilon_n(1d_{5/2})$ and take its value at $Z = 40$ to be $\Delta\varepsilon^0_n(j)$. In Fig. 15 $\delta\Delta\varepsilon_n(j) = \Delta\varepsilon_n(j) - \Delta\varepsilon^0_n(j)$ is displayed for $j = 0g_{7/2}$ and $0h_{11/2}$. Although $\varepsilon_n(0g_{7/2})$ varies almost in parallel to $\varepsilon_n(0h_{11/2})$ in $Z \geqslant 40$ for D1S, notable Z dependence arises for M3Y-P5, in qualitative agreement with the observed single-particle levels. The tensor force has significant contribution to this behavior as in the $Z = 50$ case. More realistic than D1S in the central channels but not having the tensor force, M3Y-P4 yields $\delta\Delta\varepsilon_n(j)$ in between, which is qualitatively good but quantitatively insufficient.

For the $N = 82$ nuclei, we consider $\Delta\varepsilon_n(j) = \varepsilon_n(j) - \varepsilon_n(1f_{7/2})$, from which $\delta\Delta\varepsilon_n(j) = \Delta\varepsilon_n(j) - \Delta\varepsilon^0_n(j)$ is obtained by assuming the value at $Z = 64$ as $\Delta\varepsilon^0_n(j)$. Figure 16 shows $\delta\Delta\varepsilon_n(j)$ for $j = 0h_{9/2}$ and $0i_{13/2}$. The M3Y-P5 interaction well describes $\delta\Delta\varepsilon_n(j)$ in $Z \geqslant 64$, which is affected mainly by the occupation of $p0h_{11/2}$. However, we cannot fully reproduce the tendency in $Z < 64$, which was argued in Ref. [41], although the M3Y-P5 results of $\delta\Delta\varepsilon_n(j)$ are substantially better than those of D1S and M3Y-P4. Further investigation will be necessary.

VIII. SUMMARY AND OUTLOOK

We have developed semirealistic effective interactions to describe low-energy phenomena of nuclei. Starting from the M3Y interaction, we add a density-dependent contact force and modify several strength parameters in a phenomenological manner, whereas maintain the OPEP part in the central force. We have obtained three new parameter sets; two of them (M3Y-P3 and -P5) keep the tensor force of the M3Y-Paris interaction, and the other (M3Y-P4) has no tensor force. Basic characters of the interactions are checked by the Hartree-Fock calculations for the infinite nuclear matter and for the doubly magic nuclei. The singlet-even channels of the interactions, which are relevant to the pairing properties, are fixed from

the even-odd mass differences in the Sn isotopes, by using the Hartree-Fock-Bogolyubov calculations.

We further implement the Hartree-Fock and the Hartree-Fock-Bogolyubov calculations for spherical nuclei, applying the new interactions. Predicted shell structure depends on the effective interactions to certain extent. This may significantly affect location of the drip lines. The new semirealistic interaction M3Y-P5 correctly describes the experimental consequence that the heaviest bound oxygen is ^{24}O. We have argued location of the neutron drip line for the Ca and the Ni nuclei, and its relevance to the shell structure. Variation of the single-particle energies, particularly contribution of the tensor force to it, is a current topic. It is suggested that the tensor force as well as the OPEP part of the central force play a significant role in the magic numbers $N = 16$ and 32 in the neutron-rich region. It has been shown that the new semirealistic interactions including the tensor force, M3Y-P5 in particular, describe the variation of the single-particle levels fairly well in $Z = 50$, $N = 50$, and $N = 82$ nuclei. It is remarked that this interaction can reproduce the variation of the single-particle energy difference in the Sn isotopes without destroying the shell structure of the doubly magic nuclei.

It will be of interest to apply the semirealistic interactions to deformed nuclei and to excited states via the random-phase approximation (RPA). Both projects are in progress (for the latter, see Ref. [46]).

ACKNOWLEDGMENTS

This work is financially supported as Grant-in-Aid for Scientific Research (C), No. 19540262, by Japan Society for the Promotion of Science. Numerical calculations are performed on HITAC SR11000 at Institute of Media and Information Technology, Chiba University, at Information Technology Center, University of Tokyo, and at Information Initiative Center, Hokkaido University.

[1] D. Vautherin and D. M. Brink, Phys. Rev. C **5**, 626 (1972).
[2] J. Dechargé and D. Gogny, Phys. Rev. C **21**, 1568 (1980).
[3] T. Otsuka, T. Suzuki, R. Fujimoto, H. Grawe, and Y. Akaishi, Phys. Rev. Lett. **95**, 232502 (2005).
[4] T. Lesinski, M. Bender, K. Bennaceur, T. Duguet, and J. Meyer, Phys. Rev. C **76**, 014312 (2007).
[5] S. C. Pieper, K. Varga, and R. B. Wiringa, Phys. Rev. C **66**, 044310 (2002).
[6] P. Navratíl and B. R. Barrett, Phys. Rev. C **57**, 3119 (1998); P. Navratíl, J. P. Vary, and B. R. Barrett, Phys. Rev. C **62**, 054311 (2000).
[7] G. Hagen, T. Papenbrock, D. J. Dean, and M. Hjorth-Jensen, Phys. Rev. Lett. **101**, 092502 (2008).
[8] G. Bertsch, J. Borysowicz, H. McManus, and W. G. Love, Nucl. Phys. **A284**, 399 (1977).
[9] F. Hofmann and H. Lenske, Phys. Rev. C **57**, 2281 (1998).
[10] H. Nakada, Phys. Rev. C **68**, 014316 (2003).
[11] H. Nakada, *Proceedings of the International Symposium "A New Era of Nuclear Structure Physics*," edited by Y. Suzuki, M. Matsuo, S. Ohya, and T. Ohtsubo (World Scientific, Singapore, 2004), p. 184.
[12] H. Nakada and M. Sato, Nucl. Phys. **A699**, 511 (2002); **A714**, 696 (2003).
[13] H. Nakada, Nucl. Phys. **A764**, 117 (2006); **A801**, 169 (2008).
[14] H. Nakada, Nucl. Phys. **A808**, 47 (2008).
[15] N. Anantaraman, H. Toki, and G. F. Bertsch, Nucl. Phys. **A398**, 269 (1983).
[16] K. Suzuki, R. Okamoto, and H. Kumagai, Phys. Rev. C **36**, 804 (1987); S. C. Pieper and V. R. Pandharipande, Phys. Rev. Lett. **70**, 2541 (1993).
[17] H. A. Bethe, Annu. Rev. Nucl. Sci. **21**, 93 (1971).
[18] T. Otsuka, T. Matsuo, and D. Abe, Phys. Rev. Lett. **97**, 162501 (2006).
[19] K. Oyamatsu and K. Iida, Phys. Rev. C **75**, 015801 (2007).
[20] Particle Data Group, J. Phys. G **33**, 1 (2006).
[21] J. F. Berger, M. Girod, and D. Gogny, Comput. Phys. Commun. **63**, 365 (1991).
[22] M. W. Kirson, Nucl. Phys. **A798**, 29 (2008).
[23] S. Shlomo, M. Kolomietz, and G. Colò, Eur. Phys. J. A **30**, 23 (2006).
[24] C. Mahaux, P. F. Bortignon, R. A. Broglia, and C. H. Dasso, Phys. Rep. **120**, 1 (1985).
[25] P. Danielewicz, Nucl. Phys. **A727**, 233 (2003).
[26] C. Gaarde *et al*., Nucl. Phys. **A369**, 258 (1981); T. Suzuki, Nucl. Phys. **A379**, 110 (1982); G. Bertsch, D. Cha, and H. Toki, Phys. Rev. C **24**, 533 (1981); T. Suzuki and H. Sakai, Phys. Lett. **B455**, 25 (1999).
[27] B. Friedman and V. R. Pandharipande, Nucl. Phys. **A361**, 502 (1981).
[28] D. T. Khoa, H. S. Than, and M. Grasso, Nucl. Phys. **A722**, 92c (2003).
[29] A. Ozawa *et al*., Nucl. Phys. **A691** 599 (2001).
[30] G. D. Alkhazov, S. L. Belostotsky, and A. A. Vorobyov, Phys. Rep. **42**, 89 (1978).
[31] G. Audi and A. H. Wapstra, Nucl. Phys. **A595**, 409 (1995).
[32] R. B. Firestone *et al*., *Table of Isotopes*, 8th edition (John Wiley & Sons, New York, 1996).
[33] M. Anguiano, J. L. Egido, and L. M. Robledo, Phys. Lett. **B545**, 62 (2002).
[34] K. Rutz, M. Bender, P.-G. Reinhardt, and J. A. Maruhn, Phys. Lett. **B468**, 1 (1999).
[35] J. Dobaczewski, W. Nazarewicz, and P.-G. Reinhardt, Nucl. Phys. **A693**, 361 (2001).
[36] V. A. Khodel, V. V. Khodel, and J. W. Clark, Nucl. Phys. **A598**, 390 (1996).
[37] H. Sakurai *et al*., Phys. Lett. **B448**,180 (1999).
[38] T. Aumann, Prog. Part. Nucl. Phys. **59**, 3 (2007); S. Gales, Prog. Part. Nucl. Phys. **59**, 22 (2007); T. Motobayashi, Prog. Part. Nucl. Phys. **59**, 32 (2007).
[39] R. Broda *et al*., Phys. Rev. Lett. **74**, 868 (1995).
[40] T. Otsuka, R. Fujimoto, Y. Utsuno, B. A. Brown, M. Honma, and T. Mizusaki, Phys. Rev. Lett. **87**, 082502 (2001).
[41] J. P. Schiffer *et al*., Phys. Rev. Lett. **92**, 162501 (2004).
[42] H. Nakada, Nucl. Phys. **A722**, 117c (2003).
[43] A. Ozawa, T. Kobayashi, T. Suzuki, K. Yoshida, and I. Tanihata, Phys. Rev. Lett. **84** 5493 (2000).
[44] J. I. Prisciandaro *et al*., Phys. Lett. **B510**, 17 (2001).
[45] M. Honma, T. Otsuka, B. A. Brown, and T. Mizusaki, Phys. Rev. C **65**, 061301(R) (2002).
[46] T. Shizuma *et al*. (to be published).